Key particle properties of shells for cadmium chemisorption

Chemosphere 287 (2022) 132257

Contents lists available at ScienceDirect

Chemosphere

journal homepage: www.elsevier.com/locate/chemosphere

Key particle properties of shells for cadmium chemisorption

Suguru Nakajima, Shuntaro Araki, Ryo Sasamoto, Yasuharu Kanda, Shinya Yamanaka *

Department of Applied Sciences, Muroran Institute of Technology, 050-8585, Hokkaido, Japan

HIGHLIGHTS

- Langmuir maximum adsorbed amount for the ground surf clam shells is 633.3 mg/g.
- Grinding effectively improves cadmium adsorption.
- Chemisorption is the adsorption mechanism in the calcite and aragonite phases.
- Aragonite ratio and crystallite size effect is investigated separately.
- Aragonite ratio and crystallite size are key factors for chemisorption.

GRAPHICAL ABSTRACT

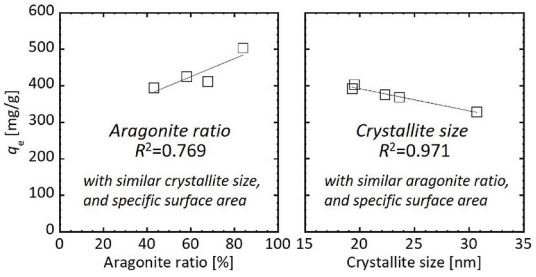

ARTICLE INFO

Handling Editor: X. Cao

Keywords:
Shells
Grinding
Cadmium ion
Chemisorption
Key particle properties

ABSTRACT

Previous studies on cadmium adsorption of calcium carbonate have found that polymorph, and, crystallinity are influential factors for adsorbing cadmium ions. The predominant factor for cadmium adsorption has yet to be elucidated because these factors are linked. To overcome this, here each factor is investigated separately. First, atmospheric grinding prepared surf clam (aragonite phase) and scallop (calcite phase) shells with similar crystallite sizes and specific surface areas. Using adsorption isotherm models, kinetics, X-ray diffraction analysis, and TEM observations, both calcite and aragonite react with cadmium to form cadmium carbonate. The chemisorption follows the adsorption mechanism reported in the literature. Based on the Langmuir isotherm model fitting, the maximum adsorbed amount for the ground surf clam shells is 633.3 mg/g, while that for scallop shells is 195.8 mg/g. Then fine surf clam shell particles with a similar specific surface area, and with a relatively wide range of the aragonite ratio, and crystallite size are prepared via a combination of grinding and a subsequent calcination process. Our experiments where one explanatory variable is changed at a time demonstrate that the polymorph ratio and crystallite size of the ground shells play key roles in the chemisorption.

1. Introduction

Pollution of water resources has a negative effect because pollutants accumulate in the human body and environment through rivers and oceans (Pourret and Bollinger, 2018). Since cadmium is resistant to rust and has an excellent malleability, it is used in various industrial applications such as batteries, pigments, plating agents, and mining (Chen et al., 2011; Acheampong et al., 2010). However, it is a toxic metal, which causes osteomalacia and impaired renal function in the human body (Liu et al., 2018). In Japan, it is known to cause Itai-Itai disease, which is a serious pollution disease (Hata, 2000). Due to its high toxicity, the World Health Organization has set an acceptable cadmium concentration in drinking water at 0.003 mg/L (Siegel, 2002).

There are various methods to remove toxic cadmium: solvent

* Corresponding author.
E-mail address: syama@mmm.muroran-it.ac.jp (S. Yamanaka).

https://doi.org/10.1016/j.chemosphere.2021.132257
Received 30 April 2021; Received in revised form 9 September 2021; Accepted 13 September 2021
Available online 16 September 2021

extraction (Petersková et al., 2012), ion exchange (Naeem et al., 2009), chemical precipitation (Bessbousse et al., 2008), filtration (Barka et al., 2012), and reverse osmosis (Kimura et al., 2004). These methods process large quantities; however, they have drawbacks, including incomplete removal of cadmium, high operating costs, long-term execution agencies, and the generation of toxic sludge (Awual et al., 2018). On the other hand, the advantages of adsorption include a high removal rate and no effective by-product generation in the treatment of dilute solutions (Wen et al., 2020). Because adsorbents are relatively expensive, more economical alternatives are necessary (Gutierrez et al., 2015; Herrero et al., 2008). Recent studies have applied a variety of cost-effective and environmentally friendly bio-adsorbents such as eggshells (Harripersadth et al., 2020), kelp (Zhao et al., 2020), peanut shells (Villar da Gam et al., 2018), wheat bran (Nouri et al., 2007), and coconut husk (Pino et al., 2006). Other studies have searched for alternatives to existing adsorbents. As an adsorbent that removes other heavy metals (lead and copper), applied research on various bio-adsorbents such as *Unio douglasiae biwae* (Michikawa et al., 2014), bamboo sawdust (Zhao et al., 2012), tobacco leaves (Yogeshwaran and Priya, 2021), and modified wheat straw (Dong et al., 2019) has been conducted.

Calcium carbonate, an abundant mineral resource, can be used to remove toxic heavy metal ions (Wen et al., 2020; Harripersadth et al., 2020; Michikawa et al., 2014; Lin et al., 2020; Chen et al., 2018; Du et al., 2012; Cubillas et al., 2005; Prieto et al., 2003; Pérez-Garrido et al., 2007; Xu et al., 2014; Van et al., 2019). Calcium carbonate has three crystal polymorphs: unstable vaterite, metastable aragonite, and the most stable calcite (Xiang et al., 2004). Because the solubility of cadmium carbonate (log $K_{sp} = -12.10$) is much lower than those of calcite (log Ksp = −8.48), aragonite (log $K_{sp} = -8.34$), and vaterite (log $K_{sp} = -7.91$) (Chen et al., 2018), cadmium carbonate should precipitate on the surface of calcium carbonate (Prieto et al., 2003; Van et al., 2019). Although vaterite is an excellent adsorbent (Lin et al., 2020; Chen et al., 2018), it is not found in nature (Lin et al., 2020). Regarding another polymorph of calcite, AFM investigations (Pérez-Garrido et al., 2007; Xu et al., 2014) confirmed epitaxial growth of cadmium carbonate on the calcite surface. For a given condition, aragonite exhibits a superior adsorption capacity than calcite to potentially toxic metals (Prieto et al., 2003; Van et al., 2019). Prieto et al. (2003) demonstrated that the epitaxial layer on the calcite armors the substrate from further dissolution. Thus, the process terminates after a small amount of cadmium is removed from the fluid.

In addition to the polymorphs of calcium carbonate, the specific surface area and crystalline size (crystallinity) are key factors for the adsorption capacity (Wen et al., 2020; Cubillas et al., 2005). Cubillas et al. (2005) demonstrated that the cadmium removal via cadmium carbonate precipitation from aragonite shells is highly efficient. They proposed that the process was favored by the larger aragonite shell surface area due to the high dissolution (Cubillas et al., 2005). Wen et al. (2020) concluded that metal carbonate precipitation from surface activated calcite is successfully enhanced using the ball mill process.

It is difficult to prepare particles so that the specific surface area, crystallite size, and polymorphs ratio can be independently changed. Because these properties are linked, changing one changes the others. There is not a report that demonstrates which factors determine the adsorption capacity. This study aims to investigate the effects of the aragonite ratio, and crystallite size on the cadmium adsorption capacity. Two types of shells, scallop shells (calcite phase) and surf clam shells (aragonite phase), are investigated. We initially confirm that the cadmium adsorption mechanism on calcite and aragonite particles with similar crystallite sizes and specific surface areas is chemisorption. Considering adsorption isotherm models, kinetics, and microstructural observations, both crystal polymorphs react with cadmium to form cadmium carbonate. Next, a combination of a particular grinding and subsequent calcination provides a relatively wide range of particle properties for surf clam shells. Thus, one explanatory variable of the particle property is successfully changed while fixing the other two particle properties. We experimentally demonstrate that the aragonite ratio and crystallite size are important factors for cadmium chemisorption.

Table 1
Particle properties and adsorbed cadmium ion amounts on ground surf clam shells (A1) and scallop shells (C1).

No.	SSA [m^2/g] [a]	Crystallite size [nm] [b]	Equilibrium concentration, C_e [mg/L]	Adsorbed amount, q_e [mg/g] [c, d]
A1	6.6 ± 0.4	32.9 ± 2.4	2.96 ± 0.40	391.3 ± 0.2
C1	6.1 ± 0.9	30.6 ± 6.7	48.3 ± 0.83	199.3 ± 4.0

[a] SSA denotes the specific surface area.
[b] Crystalline sizes of the aragonite phase of A1 and the calcite phase of C1 are calculated from the corresponding peaks at (221) and (104), respectively.
[c] Adsorption is conducted using 20 mL of a 100 mg/L cadmium solution under the optimum conditions of pH = 6.0 and an adsorption time of 180 min.
[d] Removal ratios of cadmium ions for A1 and C1 correspond to 99.6 ± 0.1% and 68.0 ± 1.1%, respectively.

2. Experimental

2.1. Materials

Surf clam shells (labeled Ax) and scallop shells (labeled C1) were provided by Maruzen Foods (Tomakomai, Japan) and Core (Sapporo, Japan), respectively. The shells were rinsed with distilled water and dried at 60 °C for one day. The raw shells were crushed using a hammer. Then the crushed shells were sieved with a 500-μm opening screen. Cadmium standard solution (1000 mg/L), tetraborate pH standard solution (pH 9.18, for pH determination), nitric acid (0.1 N, analytical grade), and sodium chloride (>99.5% purity) were purchased from Kanto Chemical (Tokyo, Japan) and used as received.

2.2. Adsorbent preparation and optimization of the adsorption conditions

Atmospheric grinding was carried out in a planetary ball mill (P-7, Fritsch, Germany). Raw shells (5.0 g) and 60.0 g of 3.0 mm yttria-stabilized zirconia ball (Nikkato, Osaka, Japan) were placed into a zirconia pot with a volume of 45 cm^3 and a diameter of 39.95 mm. The revolution speed was adjusted to 400 rpm. After grinding for 3 h, the ground shells were directly collected from the mill pot using a spoon. The samples were further dried for 24 h before using as an adsorbent. Table 1 lists the particle properties of the obtained adsorbent. Each grinding test was repeated thrice. Then the average value and standard deviation were used as the experimental data.

To determine the optimum adsorption conditions, we first investigated the influence of the cadmium solution pH and the adsorption time on the adsorption amount. The initial concentration of cadmium ion, which was prepared for a cadmium standard solution, was set to 100 mg/L. The solution pH was adjusted from 3.0 to 7.0 using a boric acid buffer solution (pH = 9.18). Then 5.0 ± 0.1 mg of the A1 or C1 sample was placed into 20 mL of the cadmium solution, and the suspension was shaken at 180 rpm for 5–240 min at a temperature of 20 °C. After 10-min centrifugation at 1205×*g*, the supernatant was filtrated using a membrane filter with a 0.1-μm pore diameter. The collected solution was diluted 10-fold with 0.1 N nitric acid.

The effect of ionic strength on the adsorption amount was then investigated using sodium chloride as a common salt. The concentration of sodium chloride was set to 0.1 mM, 1 mM, and 10 mM. Other experimental conditions were fixed at 20 °C, pH = 6.0, and 180 min.

The cadmium ion concentration of the collected solution was measured by ICP-AES (SPS7700, Seiko Instrument, Chiba, Japan). Each

Table 2
Particle properties and adsorbed characteristics.

No.	Series	Grinding time [min]	Calcination temp. [°C]	Aragonite ratio [%]	SSA [m^2/g] [a]	Crystallite size [nm] [b]	C_e [mg/L]	q_e [mg/g] [c]	Removal ratio
A2	1	3	300	83.8	7.0	35.7	25.2 ± 1.4	503.8 ± 34.4	28.9 ± 2.0
A3		3	350	67.8	5.5	46.4	20.6 ± 2.9	411.6 ± 71.1	23.6 ± 4.1
A4		3	350	58.0	5.5	32.4	21.3 ± 0.8	425.5 ± 20.4	24.4 ± 1.2
A5		3	350	43.0	4.7	35.5	19.7 ± 0.5	394.6 ± 12.1	22.6 ± 0.7
A6	2	6	–	93.0	5.9	19.5	20.2 ± 0.2	403.7 ± 3.8	23.2 ± 0.2
A7		12	–	88.8	5.2	23.6	18.5 ± 0.7	369.0 ± 17.8	21.2 ± 1.0
A8		12	–	89.3	5.5	19.3	19.6 ± 0.9	392.4 ± 22.2	22.5 ± 1.3
A9		12	–	86.9	6.3	22.3	18.8 ± 0.7	376.1 ± 17.9	21.6 ± 1.0
A10		24	–	74.3	4.9	30.7	16.4 ± 0.7	328.9 ± 18.3	18.9 ± 1.0

[a] SSA denotes the specific surface area.
[b] Crystallite size is calculated from aragonite (221) peak.
[c] Adsorption is conducted using 100 mL of a 100 mg/L cadmium solution under the optimum conditions of pH = 6.0, an adsorption time of 180 min and 0 M of sodium chloride concentration.

adsorption test was repeated thrice. Then the average value and standard deviation were used as the experimental data.

2.3. Adsorption isotherm model and adsorption kinetics

The theoretical maximum adsorption amount was evaluated by the adsorption isotherm. The initial cadmium ion concentration was set to 5–150 mg/L. Using the optimum adsorption conditions in Section 2.2, the cadmium solution pH was adjusted to 6.0, the adsorption time was 180 min, the concentration of sodium chloride was 0 M. The Langmuir, Freundlich, and Dubinin-Radushkerich isotherm models (Tran et al., 2017) were fitted to the collected data to explain the adsorption properties of the shell powder (see supporting information). The nonlinear regression analysis was carried out using KaleidaGraph (Version 4.00, Synergy Software).

The adsorption mechanism between cadmium ions and crushed shells was evaluated using the adsorption kinetic models. The reaction time was varied between 5 min and 240 min under the optimal pH condition (pH = 6.0). The nonlinear regression method was applied for pseudo-first-order (PFO) and the pseudo-second-order (PSO) equations (Ho et al., 2017) using KaleidaGraph (see supporting information).

2.4. Sample characterization

The specific surface area was measured by a nitrogen gas adsorption based on the multi-point BET method (AdsotracDN-04, Nikkiso, Osaka, Japan). Prior to measurements, the samples were degassed under a vacuum for 2 h at 200 °C to remove the adsorbed solvent molecules.

The shapes were observed using a TEM (JFM-2100 F, JEOL, Tokyo, Japan) attached with EDS (JEM-2300 T, JEOL). The acceleration voltage, probe-current, and sweep count were 200 kV, 1.00 nA, and 10, respectively. X-ray diffraction (MultiFlex-120NP, Rigaku, Japan) determined the crystal phase in a measurement range of 20°–50° at a scanning speed of 5°/min with Cu Kα. The analysis software was MDI JADE 6.0. The crystalline sizes of calcite and aragonite were calculated from the peaks of (104) and (221), respectively.

The aragonite ratio X_A [−] was calculated using the following formula (Kontoyannis and Vagenas, 2000)

$$X_A = \frac{3.157 I_{A221}}{(I_{C104} + 3.157 I_{A221})} \quad (1)$$

Where I_{A221}, and I_{C104} are the peak intensities at 2θ = 45.9° and 29.5°, respectively.

2.5. Adsorption tests using shells with several kinds of particle properties

The aragonite phase effectively adsorbs cadmium ions (Du et al., 2012; Cubillas et al., 2005). For the surf clam shells, a combination of grinding and calcination was performed to obtain various aragonite phase ratios, and crystallite sizes with a similar specific surface area. The atmospheric grinding was carried out as described in Section 2.2. After grinding for the predetermined time (3–48 h), the ground shells were collected by the bellow method and the "dry" method. Part of the collected samples was calcined at 200–350 °C using an electric furnace (FO-200, Yamato Science, Japan). Table 2 lists the particle properties of the obtained adsorbents. The aragonite ratio ranged from 43.0% to 96.1%, and the crystallite size varied from 19.3 nm to 46.4 nm. The specific surface area was fixed between 4.7 m^2/g and 7.0 m^2/g. All samples were dried for 24 h prior to use as an adsorbent.

Adsorption tests were performed in a 100-mL cadmium solution. The initial cadmium ion concentration was 100 mg/L, pH was 6.0, adsorption time was 180 min, and concentration of sodium chloride was 0 M. The other conditions were the same as those described in Section 2.2.

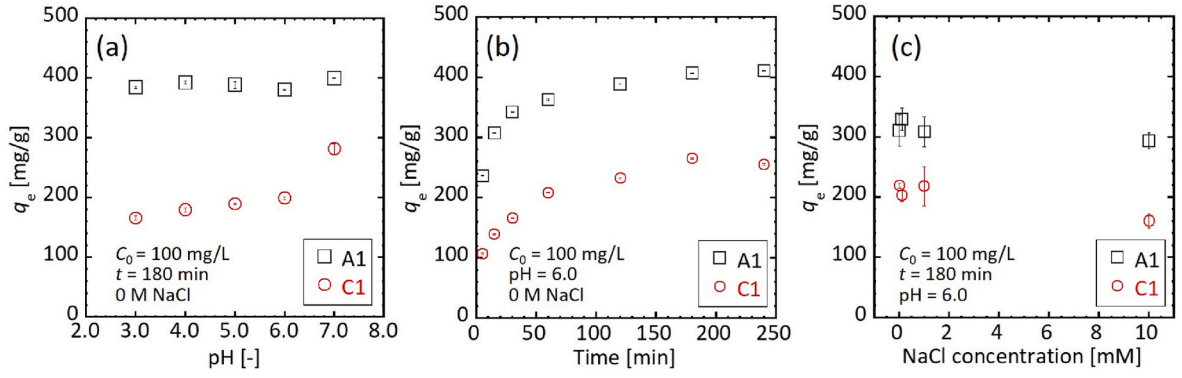

Fig. 1. Effects of (a) pH (b) adsorption time and (c) ionic strength on the adsorbed cadmium ion amount using A1 and C1 particles.

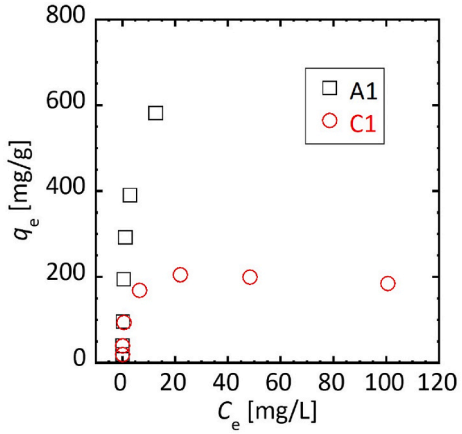

Fig. 2. Adsorption isotherm for A1 and C1 samples.

3. Results and discussion

3.1. Optimum condition for cadmium adsorption

The solution pH plays a crucial role in explaining the adsorption process between heavy metal ions and adsorbents (Abollino et al., 2003; Jeon, 2018). Because the cadmium hydroxide crystal precipitates in the alkaline region pH > 8.5 (Siswoyo et al., 2014), we initially demonstrated the adsorbed cadmium ion amount on the ground shells at pH ≤ 7.0.

Fig. 1a plots the adsorbed cadmium ion amount as a function of pH when the adsorption time is fixed to 180 min. The adsorption time was determined according to the description of the apparent equilibrium adsorption (see Fig. 1b). For the calcite phase of ground scallop shells (C1), the adsorbed amount gradually decreased as the pH became more acidic. This shift was expected because concentration of protons was increased, and the competitive adsorption decreased the cadmium cation adsorption (Abollino et al., 2003; Jeon, 2018). On the other hand, for the A1 sample, which was in the aragonite phase, the adsorbed amount did not change in the acidic region.

Prieto et al. (2003) reported cadmium ion adsorption on aragonite and calcite crystals. The surfaces of both crystal phases underwent cadmium carbonate precipitation. On the calcite surface, the precipitate was isostructural and the surface was quickly covered by a nanometer-thick layer. This epitaxial layer prevented further dissolution of the substrate. Hence, the process terminated when only a small amount of cadmium was removed from the fluid (Prieto et al., 2003). Similar to previous studies (Pérez-Garrido et al., 2007; Xu et al., 2014; Baláž et al., 2015), our results are consistent with Prieto's demonstration, indicating that the aragonite phase of A1 continuously reacts with the cadmium ion in this pH region.

Fig. 1b shows the adsorption time dependency on the adsorbed amount at pH = 6.0. During the initial stage of cadmium adsorption (5 min), A1 and C1 samples rapidly adsorbed the cadmium ion (236.6 ± 5.5 mg/g and 107.1 ± 18.4 mg/g, respectively). Within 60 min, the adsorbed amount increased to 363.2 ± 13.5 mg/g for A1 and 208.9 ± 6.1 for C1. The adsorption of both samples gradually increased over the next 120 min and approached the adsorption equilibrium at 180 min.

As shown in Fig. 1c, the adsorption amount (q_e) was slightly decreased when the salt concentration was high. The adsorption amount at 10 mM NaCl concentration was 293.7 ± 13.2 mg/g for A1, and 160.7 ± 11.7 mg/g for C1. The amount was decreased by ca. 7% for A1, and ca. 25% for C1 compared with other concentration. The initial concentration of Cd ion was 100 mg/L (equals 0.89 mM), suggesting the effect of ionic strength on the adsorption was not significant.

Based on these results, subsequent experiments were conducted with an adsorption time of 180 min, pH = 6.0, and 0 M of sodium chloride concentration.

Table 3
Comparison of the Langmuir maximum adsorption capacity (Q_e [mg/g]) of A1 and C1 toward cadmium in this study and other adsorbents in the literature.

Adsorbent	Q_e [mg/g]	Experimental conditions	Reference
A1	633.3	100 mg/L, 20 °C, 3 h, pH = 6.0	This study
C1	195.8	100 mg/L, 20 °C, 3 h, pH = 6.0	This study
eggshells	13.6	100 mg/L, room temp., 50 min, pH = 5.5	Harripersadth et al. (2020)
kelp biochar	41.7	25 mg/L, 25 °C, 10 h, pH = 6.0	Zhao et al. (2020)
peanut shells	55.4	100 mg/L, 25 °C,3 h, pH = 7.0	Villar da Gam et al., 2018
wheat bran	19.6	100 mg/L, 20 °C, 25 min, pH = 5.0	Nouri et al. (2007)
coconut shells	28.6	20 mg/L, 27 °C, 10 min, pH = 7.0	Pino et al. (2006)
sugarcane bagasse	35.5	50 mg/L, 30 °C, 1 h, pH = 6.0	Garg et al. (2008)
crayfish shell waste	93.9	500 mg/L, 30 °C, 4 h, pH = 5.0	Zhang et al. (2021)
maize straw	196.1	150 mg/L, 20 °C, 1.5 h, pH = 5.8	Guo et al. (2015)
peanut shells	188.6	200 mg/L, 25 °C, 3 h, pH = 5.0	Shan et al. (2020)
activated carbon	117.9	100 mg/L, 30 °C, 2 h, pH = 7.0	Kavand et al. (2020)

3.2. Adsorption isotherms, kinetics, and crystal structures

Using the experimental data from the 5–150 mg/L cadmium solutions (Fig. 2), the adsorption characteristics were elucidated from the Langmuir, Freundlich, and Dubinin- Radushkevich isotherm models. The calculated model parameters are show in Table S1. The Langmuir model indicated that monomolecular layer adsorption is dominant. Since there is little interaction between cadmium ions at the particle adsorption site, the maximum adsorption amount of the adsorbent can be calculated. Additionally, the Langmuir model predicted that chemical adsorption is dominant (Basu et al., 2017; De Angelis et al., 2017). By contrast, the Freundlich model predicted heterogeneous multilayer adsorption. The Freundlich model is suitable to model the adsorption of cadmium ions at low concentrations (Saeed et al., 2005). The Dubinin-Radushkevich model was developed to explain the effect of a porous adsorbent structure (Borhan and Yusuf, 2020).

From the Langmuir fitting (see Table S1), the values correlation coefficient, R^2, for A1 and C1 were 0.994 and 0.991, respectively, indicating a strong correlation with the Langmuir model. On the other hand, the R^2 values of A1 and C1 from the Freundlich fitting were 0.966 and 0.920, and those from Dubinin-Radushkevich were 0.962 and 0.970, respectively. The Freundlich and Dubinin-Radushkevich fitting had lower correlations than that of the Langmuir fitting. Van et al. (2019) reported cadmium adsorption onto aragonite bio-sorbent under an initial concentration range of 29.4–193 mg/L. They found that the isotherm was classified as an L-type without a strict plateau and concluded that cadmium had a strong affinity for the aragonite surface. Since a cadmium standard solution was used in our experiments, the upper limit of the cadmium solution was 150 mg/L. In this initial cadmium concentration range of 5–150 mg/L, the saturated adsorption might be difficult to visualize.

The maximum adsorbed amount q_m of A1 was 633.3 mg/g, which is 3.2 times larger than that of C1 (195.8 mg/g) (Table S1). This is consistent with the differences seen in Fig. 1a and the related discussion in section 3.1. That is, the aragonite phase of A1 continuously reacted with cadmium ion, while the reaction was completed on the C1 (calcite phase) surface. The same result has been reported elsewhere (Prieto

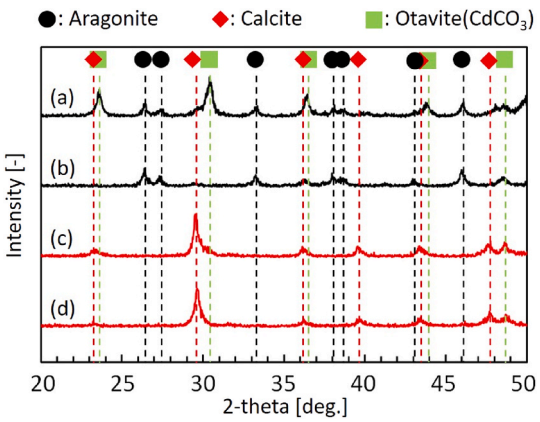

Fig. 3. XRD patterns of A1 (a) after and (b) before adsorption test, and C1 (c) after and (d) before adsorption.

et al., 2003; Van et al., 2019).

It should be noted that these maximum adsorbed amounts are relatively high compared with previous research (Table 3). Grinding effectively improved the amount of cadmium adsorption.

The time-dependent nature of the cadmium adsorption shown in Fig. 1b demonstrated that adsorption occurred rapidly within 60 min and then gradually progressed towards equilibrium. Saeed et al. (2005), Panda et al. (2007), Ifthikar et al. (2017), and Qi et al. (2017) investigated that the adsorption kinetics by using PFO rate, and PSO rate.

Two kinds of kinetic models, PFO and PSO, were applied to the A1 and C1 data. Table S3 shows the fitting results for the two models. The PSO model displayed an excellent correlation with the experimental data of A1 (R2 = 0.977) and C1 (R^2 = 0.955) compared with the PFO model (R^2 = 0.876 for A1 and 0.888 for C1).

Fig. 3 shows the crystal structures before and after the adsorption of the A1 and C1 samples. The XRD patterns of both samples contained cadmium carbonate. The main peaks of the A1 sample after adsorption shifted from aragonite to cadmium carbonate, indicating that chemical adsorption is the dominant mechanism. This is similar to the literature (Du et al., 2012; Prieto et al., 2003; Ifthikar et al., 2017). However, only small peaks of cadmium carbonate were observed in the C1 sample after adsorption since the inner calcite phase remained because the calcite–cadmium ion reaction occurred on the surface (Prieto et al., 2003).

Fig. 4 depicts typical TEM images of before (Fig. 4, A1; Fig. 4b, C1) and after cadmium adsorption (Fig. 4c, A1; Fig. 4d, C1). Prior to adsorption, both A1 and C1 particles had rounded shapes. The secondary particles consisted of primary particles 30–50 nm in size (magnified images in Fig. 4a and b), which corresponded to their crystallite size (see Table 1). After the adsorption tests, particles with a rhombohedral shape were clearly observed in Fig. 4c and d. The EDS mapping (Fig. 4e and f) of the rhombohedral particles confirmed the presence of cadmium and calcium. The calcium carbonate reacted with cadmium to form $CdCO_3$.

3.3. Key factors of shell properties for cadmium chemisorption

To determine the key factors of cadmium chemisorption on the shell particles, linear regression analysis was performed using the ground surf shells with several different particle properties (Table 2). In the experiment, two properties were fixed while one was varied. That is, the explanatory variable in series 1, and 2 were the aragonite ratio, and crystalline size, respectively. The aragonite ratio in series 1 varied 43.0–83.8% (4.7–7.0 m^2/g of the specific surface area and 32.4–46.4 nm of crystallite size), and the crystallite size in series 2 varied 19.3–30.7 nm (74.3–93.0% aragonite ratio and 4.9–6.3 m^2/g specific surface area).

Fig. 5 shows the effects of the aragonite ratio, crystallite size, and specific surface area on the cadmium adsorption. The correlation coefficients R^2 in series 1 and 2 were 0.769 and 0.971, respectively.

As mentioned in Sections 3.1, and 3.2, quick chemisorption is the mechanism for the surface reaction on both surf clam and scallop shells.

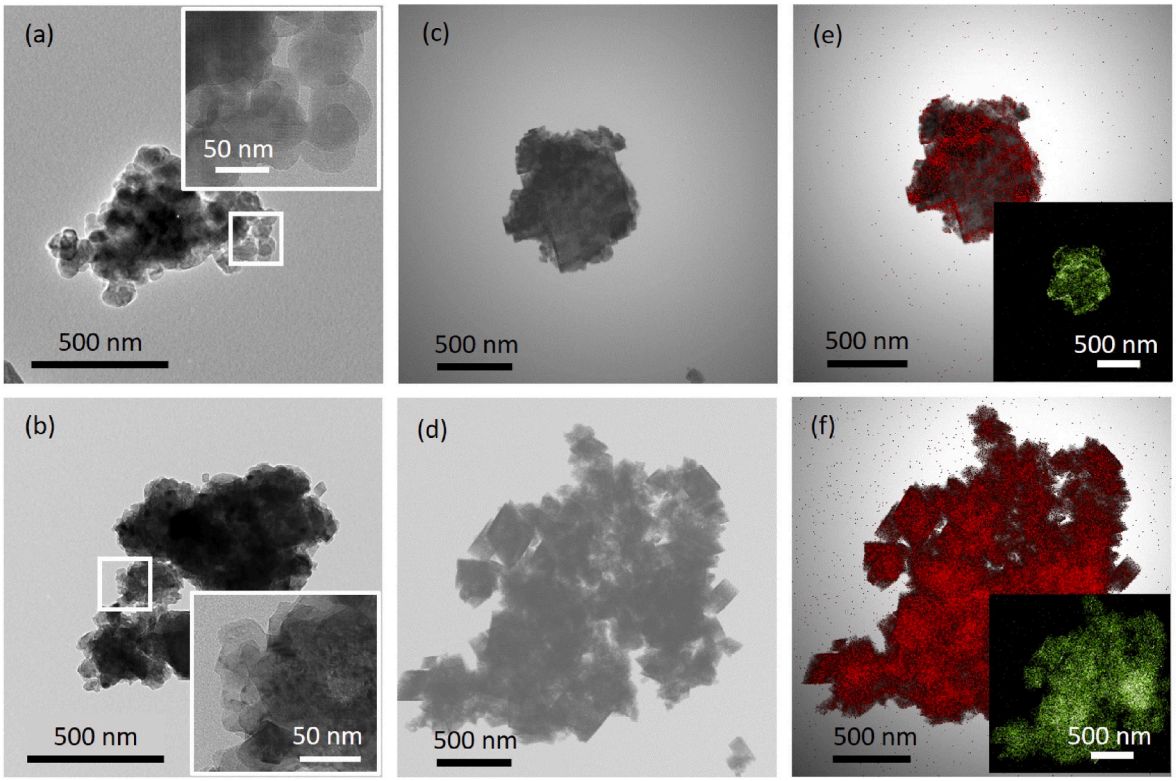

Fig. 4. Typical TEM images before (a, A1; b, C1) and after cadmium adsorption (c, A1; d, C1). EDS mapping for cadmium (e, A1; f, C1) after adsorption. Inset is a calcium image.

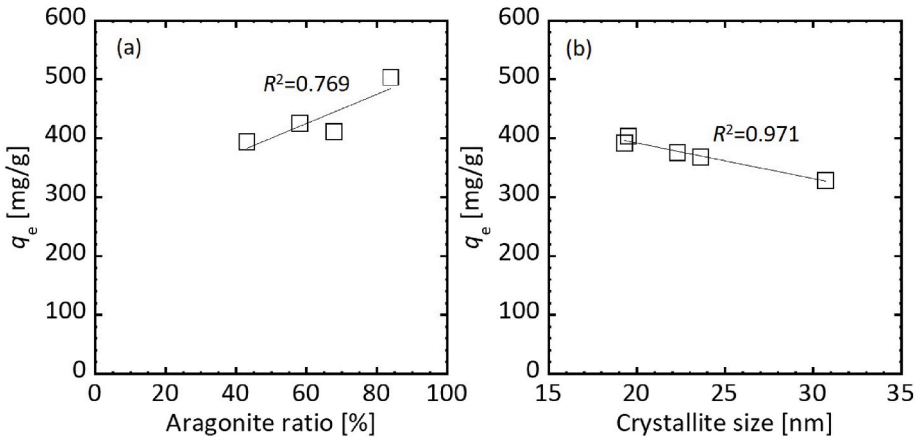

Fig. 5. Adsorbed amount of cadmium as a function of (a) aragonite ratio, and (b) crystallite size of the surf clam shell particles with a similar specific surface area.

The reaction of aragonite with cadmium ions continuously progressed. By contrast, once the reaction was completed on the surface of calcite phase, a further chemical reaction did not occur. Thus, the adsorbed cadmium amount increased as the aragonite ratio increased (Fig. 5a). Fig. 5b clearly depicts the relationship between the crystalline size and adsorbed amount. The smaller the crystalline size, the larger the adsorbed amount. A smaller crystalline size should have a lower crystallinity, indicating that a large surface energy accelerates the chemisorption. Liu et al. (2019) reported that the adsorption increased with the crystallinity reduction due to the enhanced affinity between the adsorbent and the adsorbate.

For ground shells, the aragonite ratio and crystallite size were key factors for cadmium chemisorption.

4. Conclusion

Based on the Langmuir model, the maximum adsorbed cadmium amounts were 633.3 mg/g for the ground surf clam and 195.8 mg/g for scallop shell particles. Compared to previous studies, the absorbed amount is relatively high, demonstrating that grinding can effectively enhance cadmium adsorption.

Similarly, ground surf clam shells were prepared with several kinds of particle properties. The explanatory variables for series 1, and 2 were the aragonite ratio (43–83.8%), and crystalline size (19.3–30.7 nm), respectively. The adsorbed amount of cadmium linearly increased as the aragonite ratio increased or the crystallite size decreased. The aragonite ratio and crystallite size were key factors for cadmium chemisorption.

Declaration of competing interest

The authors declare that they have no known competing financial interests or personal relationships that could have appeared to influence the work reported in this paper.

Acknowledgments

This work was supported by JSPS KAKENHI (Grant Number JP19K05117).

Appendix A. Supplementary data

Supplementary data to this article can be found online at https://doi.org/10.1016/j.chemosphere.2021.132257.

References

Abollino, O., Aceto, M., Malandrino, M., Sarzanini, C., Mentasti, E., 2003. Adsorption of heavy metals on Na-montmorillonite. Effect of pH and organic substances. Water Res. 37, 1619–1627.

Acheampong, M.A., Meulepas, R.J.W., Lens, P.N.L., 2010. Removal of heavy metals and cyanide from gold mine wastewater. J. Chem. Technol. Biotechnol. 85, 590–613.

Awual, Md R., Khraisheh, M., Alharthi, N.H., Luqman, M., Islam, A., Karim, M.R., Rahman, M.M., Khaleque, Md A., 2018. Efficient detection and adsorption of cadmium(II) ions using innovative nano-composite materials. Chem. Eng. J. 343, 118–127.

Baláž, M., Bujňáková, Z., Baláž, P., Zorkovská, A., Danková, Z., Briančin, J., 2015. Adsorption of cadmium(II) on waste biomaterial. J. Colloid Interface Sci. 454, 121–133.

Barka, N., Ouzaouit, K., Abdennouri, M., El Makhfouk, M., Qourzal, S., Assabbane, A., Ait-Ichou, Y., Nounah, A., 2012. Kinetics and equilibrium of cadmium removal from aqueous solutions by sorption onto synthesized hydroxyapatite. Desal. Water Treat. 43, 8–16.

Basu, M., Guha, A.K., Ray, L., 2017. Adsorption behavior of cadmium on husk of lentil. Process Saf. Environ. Protect. 106, 11.

Bessbousse, H., Rhlalou, T., Verchère, J.-F., Lebrun, L., 2008. Removal of heavy metal ions from aqueous solutions by filtration with a novel complexing membrane containing poly(ethyleneimine) in a poly(vinyl alcohol) matrix. J. Membr. Sci. 307, 249–259.

Borhan, A., Yusuf, S., 2020. Activation of rubber-seed shell waste by malic acid as potential CO_2 removal: isotherm and kinetics studies. Materials 13, 4970.

Chen, L., Lü, L., Shao, W., Luo, F., 2011. Kinetics and equilibria of Cd(II) adsorption onto a chemically modified lawny grass with H[BTMPP]. J. Chem. Eng. Data 56, 1059–1068.

Chen, Y.-Y., Yu, S.-H., Jiang, H.-F., Yao, Q.-Z., Fu, S.-Q., Zhou, G.-T., 2018. Performance and mechanism of simultaneous removal of Cd(II) and Congo red from aqueous solution by hierarchical vaterite spherulites. Appl. Surf. Sci. 444, 224–234.

Cubillas, P., Köhler, S., Prieto, M., Causserand, C., Oelkers, E.H., 2005. How do mineral coatings affect dissolution rates? An experimental study of coupled $CaCO_3$ dissolution–$CdCO_3$ precipitation. Geochem. Cosmochim. Acta 69, 5459–5476.

De Angelis, G., Medeghini, L., Conte, A.M., Mignardi, S., 2017. Recycling of eggshell waste into low-cost adsorbent for Ni removal from wastewater. J. Clean. Prod. 164, 1497–1506.

Dong, J., Du, Y., Duyu, R., Shang, Y., Zhang, S., Han, R., 2019. Adsorption of copper ion from solution by polyethylenimine modified wheat straw. Bioresour. Technol. Rep. 6, 96–102.

Du, Y., Zhu, L., Shan, G., 2012. Removal of Cd^{2+} from contaminated water by nano-sized aragonite mollusk shell and the competition of coexisting metal ions. J. Colloid Interface Sci. 367, 378–382.

Garg, U., Kaur, M.P., Jawa, G.K., Sud, D., Garg, V.K., 2008. Removal of cadmium (II) from aqueous solutions by adsorption on agricultural waste biomass. J. Hazard Mater. 154, 1149–1157.

Guo, H., Zhang, S., Kou, Z., Zhai, S., Ma, W., Yang, Y., 2015. Removal of cadmium(II) from aqueous solutions by chemically modified maize straw. Carbohydr. Polym. 115, 177–185.

Gutierrez, C., Hansen, H.K., Hernandez, P., Pinilla, C., 2015. Biosorption of cadmium with brown macroalgae. Chemosphere 138, 164–169.

Harripersadth, C., Musonge, P., Isa, Y.M., Morales, M.G., Sayago, A., 2020. The application of eggshells and sugarcane bagasse as potential biomaterials in the removal of heavy metals from aqueous solutions. S. Afr. J. Chem. Eng. 34, 142–150.

Hata, A., 2000. The social history of the Itai-itai disease. Jpn. Accoc. Environ. Sociology 6, 39–54.

Herrero, R., Lodeiro, P., Rojo, R., Ciorba, A., Rodríguez, P., Sastre de Vicente, M.E., 2008. The efficiency of the red alga Mastocarpus stellatus for remediation of cadmium pollution. Bioresour. Technol. 99, 4138–4146.

Ho, S.-H., Chen, Y.-D., Yang, Z.-K., Nagarajan, D., Chang, J.-S., Ren, N.-Q., 2017. High-efficiency removal of lead from wastewater by biochar derived from anaerobic digestion sludge. Bioresour. Technol. 246, 142–149.
Ifthikar, J., Wang, J., Wang, Q., Wang, T., Wang, H., Khan, A., Jawad, A., Sun, T., Jiao, X., Chen, Z., 2017. Highly efficient lead distribution by magnetic sewage sludge biochar: sorption mechanisms and bench applications. Bioresour. Technol. 238, 399–406.
Jeon, C., 2018. Adsorption behavior of cadmium ions from aqueous solution using pen shells. J. Ind. Eng. Chem. 58, 57–63.
Kavand, M., Eslami, P., Razeh, L., 2020. The adsorption of cadmium and lead ions from the synthesis wastewater with the activated carbon: optimization of the single and binary systems. J. Water Proc. Eng. 34, 101151.
Kimura, K., Toshima, S., Amy, G., Watanabe, Y., 2004. Rejection of neutral endocrine disrupting compounds (EDCs) and pharmaceutical active compounds (PhACs) by RO membranes. J. Membr. Sci. 245, 71–78.
Kontoyannis, C.G., Vagenas, N.V., 2000. Calcium carbonate phase analysis using XRD and FT-Raman spectroscopy. Analyst 125, 251–255.
Lin, P.-Y., Wu, H.-M., Hsieh, S.-L., Li, J.-S., Dong, C., Chen, C.-W., Hsieh, S., 2020. Preparation of vaterite calcium carbonate granules from discarded oyster shells as an adsorbent for heavy metal ions removal. Chemosphere 254, 126903.
Liu, F.-F., Liu, G.-Z., Zhu, Z.-L., Wang, S.-C., Zhao, F.-F., 2019. Interactions between microplastics and phthalate esters as affected by microplastics characteristics and solution chemistry. Chemosphere 214, 688–694.
Liu, X., Zhong, L., Meng, J., Wang, F., Zhang, J., Zhi, Y., Zeng, L., Tang, X., Xu, J., 2018. A multi-medium chain modeling approach to estimate the cumulative effects of cadmium pollution on human health. Environ. Pollut. 239, 308–317.
Michikawa, K., Watanabe, T., Toyohara, M., Sato, A., Toyohara, H., 2014. Development of lead adsorbent using the shell of Unio douglasiae biwae Kobelt. Nippon Suisan Gakkaishi 80, 589–593.
Naeem, A., Siddique, M.T., Mustafa, S., Kim, B., Dilara, Y., 2009. Cation exchange removal of Pb from aqueous solution by sorption onto NiO. J. Hazard Mater. 168, 364–368.
Nouri, L., Ghodbane, I., Hamdaoui, O., Chiha, M., 2007. Batch sorption dynamics and equilibrium for the removal of cadmium ions from aqueous phase using wheat bran. J. Hazard Mater. 149, 115–125.
Panda, G.C., Das, S.K., Bandopadhyay, T.S., Guha, A.K., 2007. Adsorption of nickel on husk of Lathyrus sativus: behavior and binding mechanism. Colloids Surf., B 57, 135–142.
Pérez-Garrido, C., Fernández-Díaz, L., Pina, C.M., Prieto, M., 2007. In situ AFM observations of the interaction between calcite surfaces and Cd-bearing aqueous solutions. Surf. Sci. 601, 5499–5509.
Petersková, M., Valderrama, C., Gibert, O., Cortina, J.L., 2012. Extraction of valuable metal ions (Cs, Rb, Li, U) from reverse osmosis concentrate using selective sorbents. Desalination 286, 316–323.
Pino, G.H., de Mesquita, L.M.S., Torem, M.L., Pinto, G.A.S., 2006. Biosorption of cadmium by green coconut shell powder. Miner. Eng. 19, 380–387.
Pourret, O., Bollinger, J.C., 2018. Heavy metal" - what to do now: to use or not to use? Sci. Total Environ. 610–611, 419–420.
Prieto, M., Cubillas, P., Fernández-Gonzalez, Á., 2003. Uptake of dissolved Cd by biogenic and abiogenic aragonite: a comparison with sorption onto calcite. Geochem. Cosmochim. Acta 67, 3859–3869.
Qi, F., Yan, Y., Lamb, D., Naidu, R., Bolan, N.S., Liu, Y., Ok, Y.S., Donne, S.W., Semple, K. T., 2017. Thermal stability of biochar and its effects on cadmium sorption capacity. Bioresour. Technol. 246, 48–56.
Saeed, A., Iqbal, M., Akhtar, M.W., 2005. Removal and recovery of lead(II) from single and multimetal (Cd, Cu, Ni, Zn) solutions by crop milling waste (black gram husk). J. Hazard Mater. 117, 65–73.
Shan, R., Shi, Y., Gu, J., Wang, Y., Yuan, H., 2020. Single and competitive adsorption affinity of heavy metals toward peanut shell-derived biochar and its mechanisms in aqueous systems. Chin. J. Chem. Eng. 28, 1375–1383.
Siegel, F.R., 2002. Environmental Geochemistry of Potentially Toxic Metals. Springer, Berlin, Heidelberg.
Siswoyo, E., Mihara, Y., Tanaka, S., 2014. Determination of key components and adsorption capacity of a low cost adsorbent based on sludge of drinking water treatment plant to adsorb cadmium ion in water. Appl. Clay Sci. 97–98, 146–152.
Tran, H.N., You, S.-J., Hosseini-Bandegharaei, A., Chao, H.-P., 2017. Mistakes and inconsistencies regarding adsorption of contaminants from aqueous solutions: a critical review. Water Res. 120, 88–116.
Van, H.T., Nguyen, L.H., Nguyen, V.D., Nguyen, X.H., Nguyen, T.H., Nguyen, T.V., Vigneswaran, S., Rinklebe, J., Tra, H.N., 2019. Characteristics and mechanisms of cadmium adsorption onto biogenic aragonite shells-derived biosorbent: batch and column studies. J. Environ. Manag. 241, 535–548.
Villar da Gam, B.M., do Nascimento, G.E., Sales, D.C.S., Rodríguez-Díaz, J.M., de Menezes Barbosa, C.M.B., Duarte, M.M.M.B., 2018. Mono and binary component adsorption of phenol and cadmium using adsorbent derived from peanut shells. J. Clean. Prod. 201, 219–228.
Wen, T., Zhao, Y., Zhang, T., Xiong, B., Hu, H., Zhang, Q., Song, S., 2020. Selective recovery of heavy metals from wastewater by mechanically activated calcium carbonate: inspiration from nature. Chemosphere 246, 125842.
Xiang, L., Xiang, Y., Wen, Y., Wei, F., 2004. Formation of $CaCO_3$ nanoparticles in the presence of terpineol. Mater. Lett. 58, 959–965.
Xu, M., Kovarik, L., Arey, B.W., Felmy, A.R., Rosso, K.M., Kerisit, S., 2014. Kinetics and mechanisms of cadmium carbonate heteroepitaxial growth at the calcite surface. Geochem. Cosmochim. Acta 134, 221–233.
Yogeshwaran, V., Priya, A.K., 2021. Adsorption of lead ion concentration from the aqueous solution using tobacco leaves. Mater. Today: Proc. 37, 489–496.
Zhang, D., Zhang, K., Hu, X., He, Q., Yan, J., Xue, Y., 2021. Cadmium removal by $MgCl_2$ modified biochar derived from crayfish shell waste: batch adsorption, response surface analysis and fixed bed filtration. J. Hazard Mater. 408, 124860.
Zhao, N., Li, B., Huang, H., Lv, X., Zhang, M., Cao, L., 2020. Modification of kelp and sludge biochar by TMT-102 and NaOH for cadmium adsorption. J. Taiwan Inst. Chem. Eng. 116, 101–111.
Zhao, X.-T., Zeng, T., Li, X.-Y., Hu, A.J., Gao, H.-W., Xie, Z., 2012. Modeling and mechanism of the adsorption of copper ion onto natural bamboo sawdust. Carbohydr. Polym. 89, 185–192.